Chinese Chemical Letters 36 (2025) 110719

Contents lists available at ScienceDirect

Chinese Chemical Letters

journal homepage: www.elsevier.com/locate/cclet

# Boosting the first C–H bond activation of propane on rod-like V/$CeO_2$ catalyst by photo-assisted thermal catalysis

Xiangyang Ji[a], Yishuang Chen[a], Peng Zhang[b], Shaojia Song[c], Jian Liu[a,*], Weiyu Song[a,*]

[a] State Key Laboratory of Heavy Oil Processing, China University of Petroleum, Beijing 102249, China
[b] Petrochemical Research Institute, PetroChina Company Limited, Beijing 102206, China
[c] State Key Laboratory of Clean and Efficient Coal Utilization, Taiyuan University of Technology, Taiyuan 030024, China

ARTICLE INFO

*Article history:*
Received 23 October 2024
Revised 2 December 2024
Accepted 3 December 2024
Available online 3 December 2024

*Keywords:*
Propane dehydrogenation
Facet engineering
Photothermal effect
Electrons transfer
Reaction kinetics

ABSTRACT

Crystalized $CeO_2$ structures were typically considered potential photocatalysts due to their great capacity to alter the active sites' size and ability to absorb light. However, the controllable fabrication of well-defined hierarchical structures of $CeO_2$ with high reactive facets is significant and challenging. Herein, a series of $CeO_2$ supports including hierarchical flower-like (F-$CeO_2$), ball-like (B-$CeO_2$), cube-like (C–$CeO_2$), and rod-like $CeO_2$(R-$CeO_2$) supports were prepared by hydrothermal method (B-$CeO_2$, R-$CeO_2$ and C–$CeO_2$) or ice-bath method (F-$CeO_2$) respectively. V atoms were selected as the active atoms and loaded on these supports. Their structure-activity relationship in photo-assisted thermal propane dehydrogenation (PTPDH) was investigated systematically. The samples were characterized by X-ray diffraction, scanning electron microscopy, transmission electron microscopy, $N_2$ adsorption-desorption isotherms, and Fourier transform infrared spectrum. Results show that R-$CeO_2$ support exhibits the biggest surface area thus achieving the best dispersion of $VO_x$ species. UV–vis spectrum and photoluminescence spectrum indicate that V/F-$CeO_2$ has the best light adsorption property and V/R-$CeO_2$ has the best carrier migration capacity. The activity tests demonstrate that the V/R-$CeO_2$ has the largest net growth rate and the V/F-$CeO_2$ has the biggest relative growth ratio. Furthermore, the non-thermal effect was confirmed by the kinetic method, which lowers the propane reaction orders, selectively promoting the first C–H bond activation. The light radiation TPSR experiment confirmed this point. DFT calculations show a good linear relationship between the energy barrier and the exchanged electron number. It inspires the design of high-reactive facets for boosting the intrinsic activity of the C–H bond in photo-assisted thermal chemical processes.



Propylene is a significant raw material for producing various chemicals, such as polypropene, acrylic acid, acrylonitrile, octanol, butanol, and propene oxide [1]. However, the ever-increasing demand for propylene poses a serious challenge in meeting the supply and demand gap. Propane dehydrogenation (PDH), which can effectively convert propane into propylene with high selectivity and stability, has gained much attention due to its great capacity to mitigate the tense demand for propylene, providing a promising route compared to the traditional petroleum-based routes [2].

However, the high reaction temperature (typically >650 °C) poses a new challenge in catalyst design [3–5]. The sintering of metal active sites always results in poor catalytic activity and stability. It is essential to develop new chemical processes to reduce energy consumption and increase propylene yield. Solar energy is a kind of green and pollution-free energy, showing a significant advantage in saving fossil fuels [6]. The well-designed catalyst can effectively absorb the light radiation, and the photo-generated carriers would separate into hot electrons and holes, which can be involved in the oxidation reaction and reduction reaction respectively [7,8]. However, exclusive energy input of light cannot effectively activate the C–H bond due to its strong activation constraints (~420 kJ/mol).

Photo-assisted thermal catalysis can couple the phonon and photon catalyzing the chemical reactions, moreover, it could pump the metal's energy to the specific vibration mode of the adsorbate. However, to maximize the utilization of light energy, optimizing the reaction conditions is a practicable route [9,10]. For instance, Liu *et al.* [11] found that the maximum overall light enhancement can only be achieved in the optimal light intensity and reaction temperature. The author claims the non-thermal effect has a close relationship with the light intensity and reaction tem-

* Corresponding authors.
*E-mail addresses:* liujian@cup.edu.cn (J. Liu), songwy@cup.edu.cn (W. Song).

https://doi.org/10.1016/j.cclet.2024.110719
1001-8417/

perature, while the photo-to-thermal effect is more complicated. Linic *et al.* [12,13] also found that a certain temperature would afford electron momentum, which is conducive to the generation of electron-hole pairs. The above examples indicate coupling the phonons and photos could effectively pump metal's energy to one specific vibration mode of adsorbate, thus achieving a high energy utilization in photo-assisted thermal catalysis.

Besides optimizing the reaction conditions, another point is to construct a well-designed catalyst. The elaborate control facets of the catalyst have a close relationship with its optical and textural properties [14–19]. For instance, Liu *et al.* [20] found that $CeO_2$ morphology strongly affects $NbO_x$–$CeO_2$ interactions and structures of $NbO_x/CeO_2$ catalysts, the 0.6Nb/r-$CeO_2$–500 is most active in catalyzing low-temperature ODHP reaction. Gong *et al.* [21] also found that the $VO_3/CeO_2(111)$ catalyst created new empty localized states that are mainly constituted of O 2p orbitals of the ceria-supported $VO_3$ species, which were determined to be crucial for the cleavage of the first C–H bond of the propane molecule. The light absorbance capacity of $CeO_2$ also strongly depends on its morphology, such as the sheet $CeO_2$ has better photochemical properties due to its bigger surface [22], which can provide more active sites to interact with light radiation. However, the above different methods have been proven effective in optimizing the optical properties and regulating C—H bond activation in PDH reactions. The elaborate control of the morphology of $CeO_2$ crystallites, the V atom's location on certain facets, and the structure-activity relationship, are still not systematically investigated in the photo-assisted thermal propane dehydrogenation process.

Herein, we constructed four supports with different morphologies and systematically investigated their structure-activity relationship. The monomeric $VO_x$ species were successfully loaded on the R-$CeO_2$ support, and it achieved the biggest net growth rate. The F-$CeO_2$ catalyst has the highest growth ratio. The kinetic result shows the non-thermal effect dominates the net growth rate. Exclusively increasing the temperature would lower the propane adsorption and the non-thermal effect strengthens the propane adsorption and activation. The light radiation TPSR experiment indicates that light radiation selectively boosts the first C–H bond activation rather than the second C–H bond. DFT calculations indicate the monomeric $VO_x$ species would first accept electrons from the adsorbed propane to initiate the 1st C–H bond activation. When it arrives at the transitional state, the metal sites would donate their electrons to the $C_3H_7$ fragment, finally arriving at the final state. A good linear relationship between the energy barrier and the exchanged electron number was found as a good descriptor for the first time. It shows that the lower the energy barrier, the more electrons transfer. This paper emphasizes the significance of the exchanged electron number in the activation of the C–H bond, and the photo-assisted thermal catalysis method can afford more electron exchange channels to strengthen the intrinsic activity of propane dehydrogenation.

We first utilized the SEM and TEM images to investigate the morphology and lattice fringe of different $CeO_2$ supports. It can be seen that all these particles are monodisperse particles with a uniform distribution. The C–$CeO_2$ sample as shown in Fig. 1a is cube-like with an edge length of 1.2 μm and it comprises small nanoparticles, indicating the C–$CeO_2$ has a rough surface [23]. The B-$CeO_2$ sample in Fig. 1b shows poor agglomeration among the particles. Its distribution in size is homogeneous and the shape appears rounded. According to past reports, van der Waal's force is responsible for the formation of $CeO_2$ agglomerates, which also can be seen in Fig. 1c, the flower-like $CeO_2$ support comprised of the packed $CeO_2$ pillar with a diameter of about 10 μm, the agglomeration of the pillar makes the flower-like support has a bigger surface area (29.8 $cm^2/g$) than the C–$CeO_2$ (7.1 $cm^2/g$), but it is lower

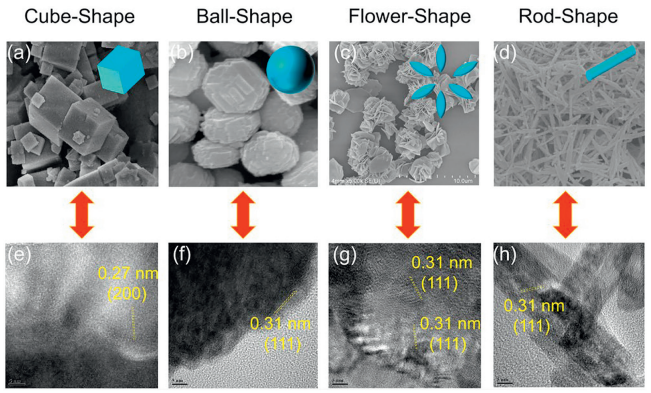


**Fig. 1.** The SEM image of the (a) C–$CeO_2$, (b) B-$CeO_2$, (c) F-$CeO_2$ and (d) R-$CeO_2$. The TEM image of the (e) C–$CeO_2$, (f) B-$CeO_2$, (g) F-$CeO_2$ and (h) R-$CeO_2$.

**Table 1**
Physicochemical properties of as-prepared catalysts.

| Sample | $S_{BET}$ ($m^2/g$) [a] | $V_P$ ($cm^3/g$) [b] | $A_{mes}$ ($m^2/g$) [c] | Band gap (eV) |
|---|---|---|---|---|
| V/C–$CeO_2$ | 7.1 | 0.047 | 10.1 | 3.2 |
| V/B-$CeO_2$ | 98.6 | 0.163 | 5.8 | 2.9 |
| V/F-$CeO_2$ | 29.8 | 0.145 | 10.3 | 2.7 |
| V/R-$CeO_2$ | 112.7 | 0.111 | 5.4 | 2.8 |

[a] BET specific surface area.
[b] Total pore volume estimated at $P/P_0 = 0.99$.
[c] Calculated by the BJH method.

than the B-$CeO_2$ (98.6 $cm^2/g$) and the R-$CeO_2$ (112.7 $cm^2/g$). The R-$CeO_2$ catalyst (Fig. 1d) is comprised of packed rods with no left particles, indicating the alkaline concentration and hydrothermal temperature are enough to completely transform the nucleation to the $CeO_2$ nanorods.

TEM images further confirmed that the four samples consisted of well-defined structures having a rectangular form. The mapping results show the successful loading of V atoms (Fig. S1 in Supporting information). The TEM images clearly show the lattice fringe of these four supports. In the C–$CeO_2$ catalyst (Fig. 1e), the lattice spacing parallel of 0.27 nm can be ascribed to the (200) plane [23,24], and the other three samples (Figs. 1f-h) have the same distance of 0.31 nm, which can be attributed to the (111) plane of $CeO_2$, implying the (111) plane is the most popular plane in the three samples.

The V atoms were loaded on the various supports by the impregnation method. The $VO_x$ polymerization has a close relationship with PDH activity. Thus, the crystal structure and morphology of different $CeO_2$ supports were investigated. In XRD patterns (Fig. 2a), all the supports exhibit typical $CeO_2$ nanocrystal peaks such as $2\theta = 28.549°$ (111), $2\theta = 33.104°$ (200), $2\theta = 47.496°$ (220) and $2\theta = 56.379°$ (311). No crystalline impurity was detected from the XRD spectrum [25]. It can be seen that V/C–$CeO_2$ has the highest crystallinity, while the other three samples show similar low crystallinity. All the samples did not show any $V_2O_5$ peaks, implying the $VO_x$ has a great dispersion on all the supports.

$N_2$ physical adsorption isotherms (Fig. 2b) were conducted to obtain the pore size, pore volume, and surface area of the four supports. The results are summarized in Table 1, it can be seen the pore size is 10.1 nm (V/C–$CeO_2$), 5.8 nm (V/B-$CeO_2$), 10.3 nm (V/F-$CeO_2$) and 5.4 nm (V/R-$CeO_2$), the pore volume is 0.04 $cm^3/g$ (V/C–$CeO_2$), 0.16 $cm^3/g$ (V/B-$CeO_2$), 0.14 $cm^3/g$ (V/C–$CeO_2$) and 0.11 $cm^3/g$ (V/R-$CeO_2$). The V/R-$CeO_2$ and V/F-$CeO_2$ both show typical IV-type curves [26], while the V/C–$CeO_2$ and V/B-$CeO_2$ both show typical II-type curves. The surface area order is V/R-$CeO_2$ (112.7 $m^2/g$) > V/B-$CeO_2$ (98.6 $m^2/g$) > V/F-$CeO_2$ (29.8 $m^2/g$) > V/C–$CeO_2$ (7.1 $m^2/g$). The V/R-$CeO_2$ has the biggest surface area,

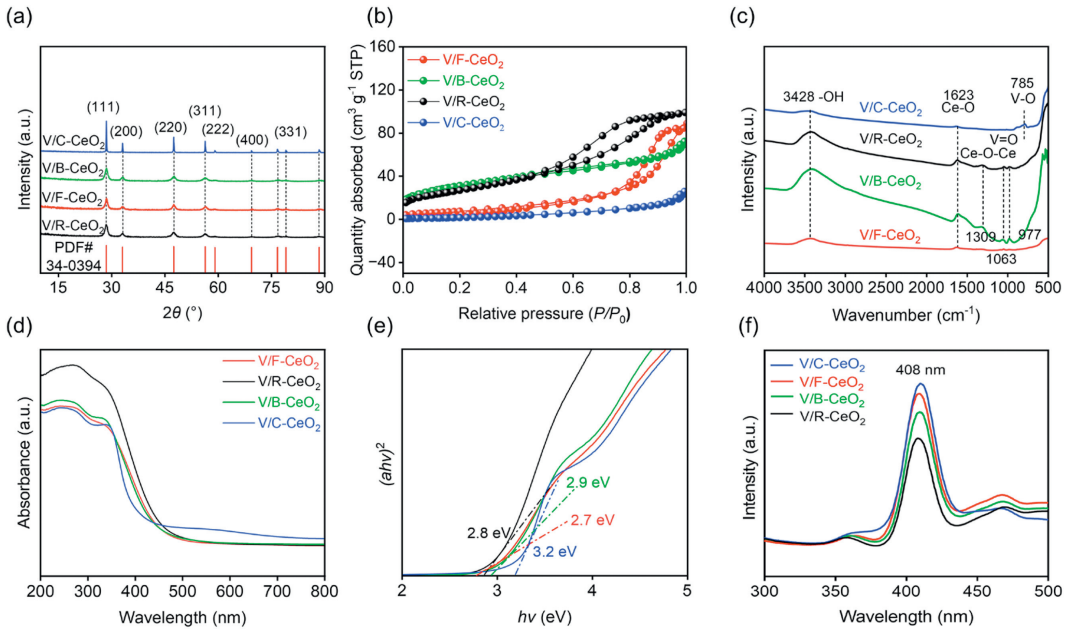


**Fig. 2.** The (a) XRD patterns, (b) $N_2$ adsorption-desorption isotherms, (c) FTIR spectrum, (d) UV–vis spectrum and (e) derived Tauc plots. (f) The photoluminescence spectrum of the V/C–$CeO_2$, V/B-$CeO_2$, V/F-$CeO_2$ and V/R-$CeO_2$ samples.

indicating the $VO_x$ has the greatest dispersion on the R-$CeO_2$ support.

The monomeric $VO_x$ species were confirmed by the FTIR (Fig. 2c). The peak at 3428 $cm^{-1}$ is attributed to the surface hydroxyl group [27]. The peaks at 1623 $cm^{-1}$ and 1312 $cm^{-1}$ are ascribed to the Ce-O bond vibration [28]. The 1044 $cm^{-1}$ and 977 $cm^{-1}$ are attributed to the V=O and V-O vibration [28,29]. The V/B-$CeO_2$ has the biggest area of the V=O peak, indicating the $VO_x$ species were polymeric on the B-$CeO_2$ support, which is consistent with its lowest surface. The 785 $cm^{-1}$ at C–$CeO_2$ is attributed to the $CeVO_4$ species, indicating the $VO_x$ species has a strong interaction with the C–$CeO_2$ support. The R-$CeO_2$ has a bigger area of the 977 $cm^{-1}$ (V-O bond), and it has a lower area of the 1044 $cm^{-1}$ (V=O bond), indicating the R-$CeO_2$ has the best dispersion of the $VO_x$ species.

The optical properties were also investigated using the UV–vis spectrum and photoluminescence spectrum. As seen in Figs. 2d and e, the light absorption capacity follows the order: V/F-$CeO_2$ (2.7 eV) > V/R-$CeO_2$ (2.8 eV) > V/B-$CeO_2$ (2.9 eV) > V/C–$CeO_2$ (3.2 eV), implying a good dispersion of $VO_x$ species conducing to the light adsorption, which may be associated with its LSPR effect [23]. The photo-generated carriers migration capacity was investigated by the photoluminescence spectrum (Fig. 2f). The V/R-$CeO_2$ has the best migration capacity, and the V/C–$CeO_2$ has the worst carrier separation ability. We speculate that a good dispersion of V species both favors light adsorption and carrier migration capacity. Following this, we conducted a series of activity evaluations and kinetic tests to confirm and elucidate the non-thermal effect.

The catalytic activity tests were conducted and the result can be seen in Fig. S2 (Supporting information). It shows the V/R-$CeO_2$ has the highest propane conversion under both dark and light conditions. We also obtained the growth ratio brought by the light radiation. It can be seen that V/F-$CeO_2$ has the highest growth ratio. The ratio order is V/F-$CeO_2$ (39.2%) > V/R-$CeO_2$ (19.8%) > V/B-$CeO_2$ (13.0%) > V/C–$CeO_2$ (5.6%). The order indicates a close relationship with the catalyst's light absorption and carrier migration capacity.

To confirm that the non-thermal effect dominates the PTPDH process instead of the photo-to-thermal effect, the TPSR experiment was conducted to investigate the $C_3H_8$ and $H_2$ signals under dark and light conditions. As shown in Fig. 3a, it shows the propane onset temperature is 331 °C without light radiation, while after the light radiation, the propane disappears quickly (~233 °C under light conditions as shown in Fig. 3b). The propylene appearance temperature is ~423 °C under dark conditions, while with the assistance of light, it reduces to ~372 °C. The above results indicate that light radiation helps the activation of propane and the generation of propylene. However, the $H_2$ onset temperature is ~240 °C no matter the conditions. This result strongly demonstrates that the light radiation would not affect the $H_2$ dissociation or H coupling process, and this reverse reaction would not strongly affect the PDH process. Thus, the rate-determined step on the V/R-$CeO_2$ is most likely the first C–H bond activation process.

Kinetic experiments were further conducted to confirm the non-thermal effect [30]. Propane reaction orders under dark or light conditions were obtained to exclude the photo-to-thermal effect. The derivation process can be found in Section 1 in Supporting information. As shown in Fig. 3c, exclusively increasing the reaction temperature would boost the propane reaction order, according to past reports [31,32], the lower the propane reaction order, the stronger the adsorption and activation of the propane molecule gets. Thus, it can be deduced that increasing the temperature would suppress the propane adsorption and activation. After the light radiation (Fig. 3d), the reaction order decreases slightly, indicating the non-thermal effect can beat the photo-to-thermal effect. Thus, the non-thermal effect would boost the propane adsorption and activation.

The apparent activation energy was obtained as shown in Fig. S3 (Supporting information). Increasing the propane flow rate would suppress its intrinsic activity. After the light radiation, the intrinsic activity would be boosted, indicating the non-thermal effect can effectively accelerate the electron transfer rate between the adsorbate and the metal centers [33,34]. The stability test (Fig. S4a in Supporting information) indicates the catalysts have good stability under light radiation conditions. Furthermore, thermogravimetry analysis (Fig. S4b in Supporting information) was conducted and it shows the PTPDH has less coke than the PDH with

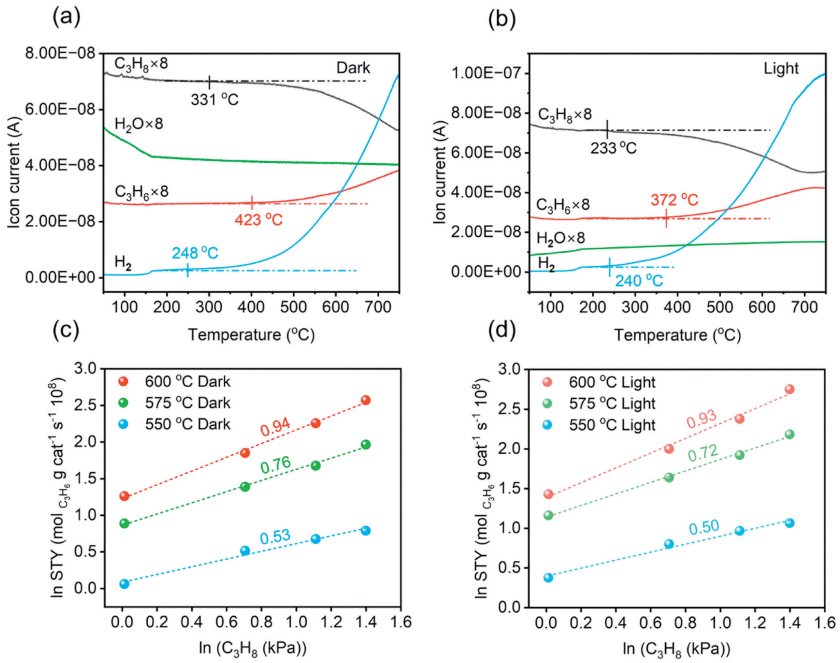


**Fig. 3.** The temperature-programmed surface reaction of propane dehydrogenation over V/R-$CeO_2$ under (a) dark or (b) light conditions. The $C_3H_8$ reaction orders of the four samples under (c) dark or (d) light conditions.

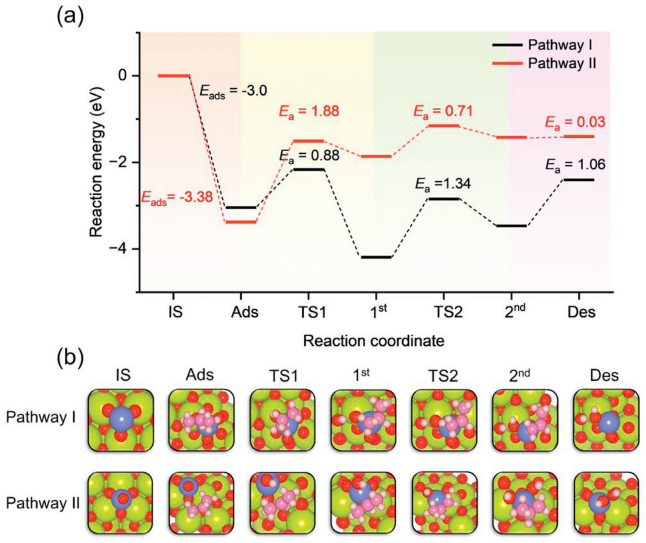


**Fig. 4.** (a) The potential energy surface of pathway I and pathway II. (b) The detailed reaction configurations in the propane dehydrogenation process.

a similar conversion of propane. Both experiments indicate the PTPDH process is more stable.

DFT calculations were conducted to investigate the detailed electronic effect on the PTPDH process [35,36]. Two reaction pathways were considered and the potential energy surface (PES) can be found in Fig. 4a. The monomeric $VO_3$ species was considered the active site in the PTPDH process and the detailed models are shown in Fig. 4b. Model I is one $VO_3$ loaded on the $CeO_2$ surface without a dangling O atom, and the model II is one $VO_3$ species loaded on the $CeO_2$ surface with a dangling O atom. Model I shows a lower energy barrier (0.88 eV) for the 1st dehydrogenation step but a higher energy barrier (1.34 eV) for the 2nd step, while model II has a higher energy barrier (1.88 eV) for the 1st dehydrogenation step and a lower energy barrier (0.71 eV) of the 2nd step. According to the Sabatier principle [37], a successful catalytic cycle in heterogeneous catalysis always originates from neither too strong nor too weak adsorption of intermediate. Thus, the higher the 1st step must accompany with the lower the 2nd step. This unbalanced kinetic condition would significantly suppress the overall PDH production.

The DOS analysis was conducted to illustrate the effect of the light radiation on the PDH as shown in Fig. S5 (Supporting information) [38]. When the propane molecule was adsorbed on the surface of model I, there was no occupation of the C and H atoms (Fig. S5a). When the first H atom was dissociated, the occupation of the C and H atoms appeared at ~−2.5 eV (Fig. S5b). Such a lower energy level rationalizes the higher energy barrier of the 2nd step. As for model II, the occupation of the C and H atoms appeared at ~−1.3 eV (Fig. S5d) and ~2.6 eV (Fig. S5e) respectively. When the first H atom was dissociated, the occupation of the C and H atoms appeared at ~−1.2 eV The higher energy level (−1.2 eV > −2.5 eV) accompanies a lower energy barrier in the 2nd step. According to the Frontier molecular orbit theory [39,40], the chemical reactivity is only decided by the relative energy level of the HOMO and LUMO of the hybrid orbits. Thus, an appropriate electronic wave function overlap confers a neither too strong nor too weak interaction between the metal atoms and adsorbate. We speculated the high energy level of C and H atoms is more favorable for the influx of electrons.

Thus, we tracked the electronic density of the metal active site within the PDH process. In pathway I, the metal center first accepts the electron to arrive at the transitional state, then releases its electrons to arrive at the 1st state (Fig. S6 in Supporting information). The electronic fluctuation of pathway I (0.6 $e^-$) is bigger than pathway II (0.1 $e^-$), indicating more electron influx lowered the energy barrier. As for the 2nd step, in pathway I, it first releases its electron to arrive at the transitional state and then releases electrons to arrive at the 2nd state. While in pathway II, the metal would accept the electrons from the adsorbate and release the electrons to arrive at the 2nd state. Pathway I has a

higher energy barrier in the 2nd step than Pathway II, which may come from the subsequent electron release behavior, leading to the metal center in an electron-deficient state. In Pathway II, the metal would first accept the electrons, the electron-rich state lowers the energy barrier of the 2nd step. In all, it can be deduced the electron can help lower the reaction barrier and boost the PDH performance.

The exchanged electron number was correlated to its energy barrier within the 1st, and the 2nd C–H bond activation or the H coupling desorption processes (Figs. S5c and f). The negative relationship indicates the more exchanged electron numbers, the lower the active energy barrier of C–H bond activation is.

In conclusion, we prepared four $CeO_2$ supports with different morphologies, a series of characterization results indicate that R-$CeO_2$ has the biggest surface area, leading to the best dispersion capacity for $VO_x$ species and good light absorption capacity. The kinetic result shows that exclusively increasing the temperature would suppress the 1st step, while light radiation can boost overall propylene production. The light radiation TPSR experiment demonstrates that light radiation selectively boosts the 1st step and thus balancing the kinetic conditions. DFT calculations indicate that light accelerates the electron transfer behavior within the 1st dehydrogenation process. More electrons were involved in the 1st step and thus lowering the reaction energy barrier. The linear relationship between the energy barrier and the exchanged electron number supports this point. This paper emphasizes the significance of the electron exchange in the activation of the C–H bond, and the photo-assisted thermal catalysis method can afford more electron exchange channels to strengthen the intrinsic activity of propane dehydrogenation.

## Declaration of competing interest

The authors declare that they have no known competing financial interests or personal relationships that could have appeared to influence the work reported in this paper.

## CRediT authorship contribution statement

**Xiangyang Ji:** Project administration, Methodology, Investigation, Formal analysis, Data curation, Conceptualization. **Yishuang Chen:** Project administration, Methodology, Data curation, Conceptualization. **Peng Zhang:** Supervision, Software, Funding acquisition. **Shaojia Song:** Methodology, Conceptualization. **Jian Liu:** Visualization, Methodology, Investigation. **Weiyu Song:** Writing – review & editing, Writing – original draft, Visualization, Conceptualization.

## Acknowledgments

We gratefully acknowledge the financial support from the National Key R&D Program of China (Nos. 2021YFA1501301, 2021YFC2901100) and the National Natural Science Foundation of China (Nos. 22178381, 22035009).

## Supplementary materials

Supplementary material associated with this article can be found, in the online version, at doi:10.1016/j.cclet.2024.110719.

## References

[1] S. Chen, X. Chang, G. Sun, et al., Chem. Soc. Rev. 50 (2021) 3315–3354.
[2] T. Yang, F. Su, D. Shi, et al., Chin. Chem. Lett. 36 (2025) 110444.
[3] L. Liu, M. Lopez-Haro, C.W. Lopes, et al., Nat. Mater. 18 (2019) 866–873.
[4] L. Liu, M. Lopez-Haro, C.W. Lopes, et al., Nat. Catal. 3 (2020) 628–638.
[5] L. Liu, M. Lopez-Haro, C.W. Lopes, et al., J. Catal. 391 (2020) 11–24.
[6] C. Gu, H. Ji, K. Xu, et al., Chin. Chem. Lett. (2024), doi:10.1016/j.cclet.2024.110565.
[7] X. Ji, Y. Ma, X. Sun, S. Song, et al., ACS Appl. Nano Mater. 6 (2023) 6354–6364.
[8] R. Zhang, H. Wang, S. Tang, et al., ACS Catal. 8 (2018) 9280–9286.
[9] X. Zhang, X. Li, D. Zhang, et al., Nat. Commun. 8 (2017) 14542.
[10] X. Li, X. Zhang, H.O. Everitt, J. Liu, Nano Lett. 19 (2019) 1706–1711.
[11] Z. Geng, Y. Yu, A.J. Offen, J. Liu, Nat. Catal. 6 (2023) 1241–1247.
[12] P. Christopher, H. Xin, A. Marimuthu, S. Linic, Nat. Mater. 11 (2012) 1044–1050.
[13] S. Linic, S. Chavez, R. Elias, Nat. Mater. 20 (2021) 916–924.
[14] W.Z. Yu, W.W. Wang, S.Q. Li, et al., J. Am. Chem. Soc. 141 (2019) 17548–17557.
[15] S. Yang, L. Gao, J. Am. Chem. Soc. 128 (2006) 9330–9331.
[16] X. Xiang, L. Wu, J. Zhu, et al., Chin. Chem. Lett. 32 (2021) 3215–3220.
[17] Y. Shan, X. Deng, X. Lu, et al., Chin. Chem. Lett. 33 (2022) 5158–5161.
[18] B. Liu, Q. Lia, X. Du, et al., J. Alloys Compd. 509 (2011) 6720–6724.
[19] Y. Mei, Y. Zhang, J. Li, et al., J. Alloys Compd. 904 (2022) 163879.
[20] Y. Liu, L. Luo, Y. Gao, W. Huang, Appl. Catal. B: Environ. 197 (2016) 214–221.
[21] C. Huang, Z.Q. Wang, X.Q. Gong, Chin. J. Catal. 39 (2018) 1520–1526.
[22] Y. Liu, Z. Shen, J. Song, et al., Chin. Chem. Lett. 31 (2020) 2747–2751.
[23] B. Feng, D. Li, J. Xiong, et al., Appl. Catal. B: Environ. 325 (2023) 122337.
[24] Y. Wang, S. Chen, J. Sun, et al., Sci. China Mater. 66 (2023) 1062–1070.
[25] B.M. Reddy, A. Khan, P. Lakshmanan, et al., J. Phys. Chem. B 109 (2005) 3355–3363.
[26] H. Ning, K. Xie, B. Jiang, et al., J. Rare Earths (2024), doi:10.1016/j.jre.2024.06.029.
[27] T. Wu, G. Liu, L. Zeng, et al., AIChE J. 63 (2017) 4911–4919.
[28] G. Qi, R.T. Yang, J. Phys. Chem. B 108 (2004) 15738–15747.
[29] M.V. Bosco, M.A. Bañares, et al., J. Mol. Catal. A: Chem. 408 (2015) 75–84.
[30] X. Li, H.O. Everitt, J. Liu, Nano Res. 12 (2019) 1906–1911.
[31] S. Song, K. Yang, P. Zhang, et al., ACS Catal. 12 (2022) 5997–6006.
[32] J. Zhu, M.-L. Yang, Y. Yu, et al., ACS Catal. 5 (2015) 6310–6319.
[33] W. Wang, Q. Song, Q. Luo, et al., Nat. Commun. 14 (2023) 2493.
[34] Z. Xiao, P. Li, H. Zhang, et al., Fuel 362 (2024) 130906.
[35] J.P. Perdew, K. Burke, M. Ernzerhof, Phys. Rev. Lett. 77 (1996) 3865.
[36] G. Henkelman, B.P. Uberuaga, H. Jónsson, J. Chem. Phys. 113 (2000) 9901–9904.
[37] Z.J. Zhao, S. Liu, S. Zha, et al., Nat. Rev. Mater. 4 (2019) 792–804.
[38] P. Wang, X. Zhang, R. Shi, et al., Nat. Commun. 15 (2024) 789.
[39] G. Klopman, J. Am. Chem. Soc. 90 (1968) 223–234.
[40] J. Yu, N.Q. Su, W. Yang, JACS Au 2 (2022) 1383–1394.